Flexible and Printed Electronics

PAPER

A seed and bridge layer method for inkjet printing of narrow traces on receding ink-substrate combinations

To cite this article: Nicholas Pratt and Pratap M Rao 2023 *Flex. Print. Electron.* **8** 045008

IOP Publishing Flex. Print. Electron. 8 (2023) 045008 https://doi.org/10.1088/2058-8585/ad1051

Flexible and Printed Electronics

PAPER

A seed and bridge layer method for inkjet printing of narrow traces on receding ink-substrate combinations

RECEIVED
28 August 2023

REVISED
2 November 2023

ACCEPTED FOR PUBLICATION
28 November 2023

PUBLISHED
7 December 2023

Nicholas Pratt and Pratap M Rao*

Department of Mechanical and Materials Engineering, Worcester Polytechnic Institute, Worcester, MA, United States of America
* Author to whom any correspondence should be addressed.

E-mail: pmrao@wpi.edu

Keywords: inkjet printing, seed and bridge layer printing, printed electronics, printed traces

Supplementary material for this article is available online

Abstract

Inkjet printing of electronic materials is of interest for digital printing of flexible electronics and sensors, but the width of the inkjet-printed lines is still large, limiting device size and performance. Decreasing the drop volume, increasing the drop spacing, and increasing the ink-substrate contact angle are all approaches by which the line width can be lowered, however these approaches are limited by the nozzle geometry, ink coalescence and bead instabilities, and contact angle hysteresis, respectively. Here we demonstrate a novel approach for stable inkjet printing of very narrow lines on ink-substrate combinations with a high contact angle, utilizing the de-wetting of the ink due to the decreased contact angle hysteresis. After printing and drying an initial layer of disconnected seed drops of silver nanoparticle ink, we print an additional layer of bridging drops of the same ink in between the dried seed drops. The bridging drops expand to touch the dried seed drops and then retract into a line, due to the pinning of the wet ink on the dried seed ink but not on the substrate, forming a continuous silver trace. The trace width is decreased from 60 μm with a traditional printing approach down to 12.6 μm with this seed-bridge approach. The electrical conductivity of the silver trace is similar to that of a conventionally printed trace. Due to poor adhesion on the print substrate, the trace was transferred to a separate polymer substrate with a simple hot-pressing procedure, which preserves the electrical conductivity of the trace.

1. Introduction

Inkjet printing of conductive inks comprising silver nanoparticles or conductive polymers in solvents has been used to print electronic circuits and sensors. Inkjet printing has the benefit of being a digital process, meaning that no mask or master pattern is required, and the design can be changed on the fly, making it ideal for research, prototyping and iteration, and low volume manufacturing. Among digital processes, it has a relatively high throughput as the number of nozzles on a printhead can be easily scaled up. Furthermore, because it is a purely additive process, there is much less waste of material and generation of hazardous waste compared to conventional subtractive printed circuit board manufacturing [1].

Strain sensors [2], gas sensors [3], sweat sensors [4], temperature sensors [5], touch sensors [6], and antibiotic sensors [7], have all been inkjet-printed, using arrays of narrow silver nanoparticle traces either as electrodes or as the active material itself. Printed silver traces onto which rigid integrated circuit and passive components have been surface-mounted have also been used to create multilayer flexible hybrid electronic devices [8]. For these sensors that are utilizing inkjet-printed interdigitated electrodes, increasing the finger density by decreasing the width of the interdigitated fingers and the gap between the fingers can improve the device performance. However, inkjet struggles with printing narrow traces with small spacing due to its relatively large linewidth and low resolution [9].

Piezoelectric inkjet printing (the most common jetting method, referred to here simply as inkjet) has a relatively large minimum achievable linewidth. 100–200 μm is achieved routinely, and linewidths down to 25 μm are achievable in optimized cases [10]. In contrast, other additive printing processes such as

electrohydrodynamic jetting can achieve linewidths down to 2 μm [11]. This small linewidth allowed printed thin film transistors to have a very small parasitic capacitance on the order of picofarads, showing how decreasing the printed linewidth of a processes can improve the performance of devices and increase its applicability. However, processes such as electrohydrodynamic inkjet and aerosol jet suffer from lower throughput due to a limited number of nozzles. In aerosol jet, this is due to geometric constraints on the printhead [12], while for electrohydrodynamic jet, it is due to 'cross-talk' between the electric fields that each nozzle must generate with the substrate to jet the drops of ink [13]. Aerosol jet also struggles with increasing material deposition speed for single nozzles, as higher flow rates tend to lead to evaporation and internal deposition in the nozzles [12]. *The objective of the present study, therefore, is to decrease the minimum linewidth possible for common piezoelectric inkjet printing.*

Inkjet-printed traces are typically made using ink-substrate combinations that have a receding contact angle (θ_R) of 0°, meaning that the ink does not recede or de-wet from a previously wetted area of the substrate. Drops are printed with a particular spacing such that the coalescence of the neighboring drops results in the formation of a continuous bead of ink, which dries into a printed trace. As the printed drops coalesce, the wet bead that they form resembles a truncated cylinder (figure 1). Because the ink does not recede, the width of the dried trace is the same as that of the truncated cylinder of wet ink. Stringer and Derby derived the dependence of the width of the truncated cylinder on the jetted drop diameter (d_0), the ink-substrate contact angle (θ) and the drop spacing (p), as shown in equations (1) and (2) [14], where β is the normalized spherical cap diameter and w is the bead width. The spherical cap diameter refers to the diameter of a truncated sphere that is formed by a drop of ink on the surface of the substrate with a contact angle θ, which is normalized by the diameter of the jetted drop in equation (1). Initially, the equilibrium contact angle was used for θ in these predictions, but later work demonstrated that the advancing contact angle (θ_A) showed better agreement with experimental results [14].

$$\beta = \left[\frac{8}{\tan\frac{\theta}{2}\left(3+\tan^2\frac{\theta}{2}\right)}\right]^{\frac{1}{3}} \tag{1}$$

$$w = \beta d_0 \sqrt{\frac{2\pi d_0}{3p\beta^2\left(\frac{\theta}{\sin^2\theta}-\frac{\cos\theta}{\sin\theta}\right)}}. \tag{2}$$

As seen from this derivation, three things can be changed to decrease the width of the bead, and hence the width of the printed line: increasing the spacing p between the drops, decreasing the diameter d_0 (or equivalently, the volume) of the printed drop, and increasing the ink-substrate contact angle θ.

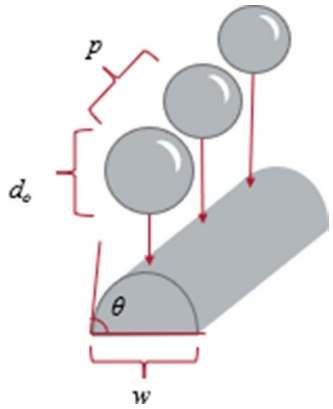

Figure 1. Dimensions of the truncated cylinder of wet ink.

Pre-patterning the substrate with micro-channels [15] or photolithographically-applied metal traces [16] can also result in decreased trace widths, but either approach removes the digital advantage of inkjet. Printing on permeable substrates can also reduce the volume of ink on the surface of the substrate, changing the expansion and drying dynamics [17]. The approach of increasing the drop spacing is limited by the drops needing to touch to coalesce and form the bead. Increasing the drop spacing from 6 μm to 10 μm has been shown to decrease trace width from around 85 μm down to 60 μm in one instance [18]. However, as the drop spacing is increased further, the drops no longer touch, and the trace becomes discontinuous [18]. By using printheads designed to jet small volumes, the volume of the truncated cylinder is decreased, again resulting in narrower linewidths [10, 11]. Work that has been done on decreasing the drop volume from 10 pl to 2 pl has resulted in the trace width decreasing from an estimated 85 μm down to 25 μm [10]. However, this approach is limited by low throughput, as these smaller drops require smaller drop spacings, meaning that a larger number of drops have to be jetted for the same line length [11]. The contact angle can be controlled by heating [18, 19], chemical treatments [20], patterning [21], or simply changing the substrate. Increasing θ from 46° to 54° has resulted in a decrease in trace width from about 48 μm to 38 μm [19]. However, methods to increase the advancing contact angle θ_A by increasing θ_{young} and $\theta_{apparent}$ (the equilibrium contact angles for smooth and rough surfaces, respectively), also tend to decrease the contact angle hysteresis (θ_A–θ_R), increasing the likelihood that θ_R will no longer be 0 [22, 23]. This means that the ink will be able to recede from previously wetted regions, i.e. de-wet the substrate. This typically happens as θ_{young} approaches 90° [23] although it also depends on other factors such as substrate roughness [22].

Using ink-substrate combinations in which $\theta_R > 0°$, when the ink can dewet the substrate, allows the drops of ink to not only recede after they have spread out after impact, but also to move around on the substrate after they have been printed, including allowing their center of mass to translate away from the position at which they were printed, during coalescence with neighboring drops. This does not typically allow for printing of stable beads, as the drops can coalesce in an undesirable manner to form large isolated drops instead of a continuous bead [24, 25].

Here, we devise a novel approach by which continuous lines can be stably inkjet-printed on substrates with high θ_A, thereby achieving narrow linewidths, even though $\theta_R \gg 0°$. The approach combines two ideas: (i) if the spacing between the printed drops is large enough that they never touch one another, they will remain as the discrete small drops until they dry and (ii) any subsequently printed ink will preferentially wet the previously-printed dry ink instead of wetting the substrate. Therefore, the approach entails printing a seed layer of discrete drops of ink far enough apart to avoid coalescence, allowing these to dry completely, and then printing subsequent drops in between these dried drops, that will wet both adjacent dried drops and recede into a line that stretches between the dried drops, forming a continuous trace.

2. Method

Agfa Prelect SPS 201 silver nanoparticle ink was printed on a polyimide substrate coated with fluorinated ethylene propylene (Kapton FN). The printing was done with a Konica Minolta KM512-SHX printhead (4 pl nominal drop volume) and a Süss Microtec LP50 printer. The jetting settings, drop volume, drop velocity, and drop images are provided in the supplementary materials table S1 and figure S1. The substrate was wiped with isopropanol and allowed to dry for 1 min before printing. All printing was done with a jetting frequency of 1000 Hz and with a 0.5 mm distance between the printhead and the substrate. Printed traces were cured in an oven at 170 °C for 30 min after printing. A ramé-hart Model 210 goniometer was used to measure the ink-substrate contact angles. A Keyence VHX-7000 4k digital microscope was used the image the traces. A KLA Tencor AlphaStep D-600 Stylus profilometer and a ZYGO Nexview NX2 optical profilometer were used to measure trace cross section profiles. For conventional prints, pads were printed over the ends of the traces with the silver ink, and the resistance was measured with a multimeter. For the seed-bridge traces, which were much narrower, electrical resistance measurements were taken through copper tapes placed over the ends of the printed traces using liquid indium–gallium eutectic to make good electrical contact. All resistance measurements were 2-terminal, without correction for contact resistance. Multiple traces were measured simultaneously and were treated as parallel resistors to calculate the resistance per length of the individual traces.

Table 1. Static, advancing (θ_A) and receding (θ_R) contact angles for Agfa 201 ink measured on PET ST505 and Kapton FN substrates at 70 °C.

Substrate	Static	Advancing	Receding
Kapton FN	77.1°	82.7°	55.4°
PET ST505	22.4°	25.0°	0°

3. Results

The static, advancing, and receding contact angles of the Agfa Prelect 201 ink were measured on two substrates—adhesion-coated polyethylene terephthalate (PET ST505), and fluorinated ethylene propylene (Kapton FN)—at 70 °C, and are shown below in table 1.

The ink has $\theta_R = 0°$ on the PET substrate, meaning that it cannot recede or de-wet this substrate. Under this condition, the adjacent drops of ink form a stable bead and we can print this ink using a conventional approach on this substrate, as shown in figure 2(a). Here, when the drop spacing is made small enough (i.e. 40 μm) that the adjacent drops overlap sufficiently, a trace with straight edges is formed. However, the ink has a relatively small $\theta_A = 25.0°$, meaning that the ink spreads out considerably on the substrate, forming a relatively wide bead. As a result, the minimum trace width is around 60 μm, which is relatively large.

In contrast, $\theta_A = 82.7°$ for the ink on the Kapton FN substrate is high, which would mean that a bead formed by this ink-substrate combination is a promising candidate for printing narrow traces. However, $\theta_R = 55.4°$ for the Kapton FN substrate means that a stable bead will not form because the ink will readily recede, i.e. de-wet the substrate, causing adjacent drops to translate laterally while coalescing into larger, separated drops. This is clearly shown in figure 2(b), in which we varied the drop spacing with which the ink was printed on Kapton FN. Drops printed with a spacing of 27.5 μm and larger are far enough apart that they do not come into contact with the adjacent drops even when they flatten and expand after impact (impact-driven expansion). Consequently, they recede without any lateral translation and dry to form separate printed dots on the substrate, at the same positions at which they were originally printed. An example of impact-driven expansion followed by de-wetting/recession is shown in figure S2 for a larger drop of the same ink on this substrate. In contrast, for drop spacings of 25.0 and 22.5 μm, the drops are sufficiently close together that they come into contact with the adjacent drop when they flatten and expand after impact. This causes 2 adjacent drops to translate laterally and coalesce into a larger cap. Similarly, drops printed with spacings of 20.0 and

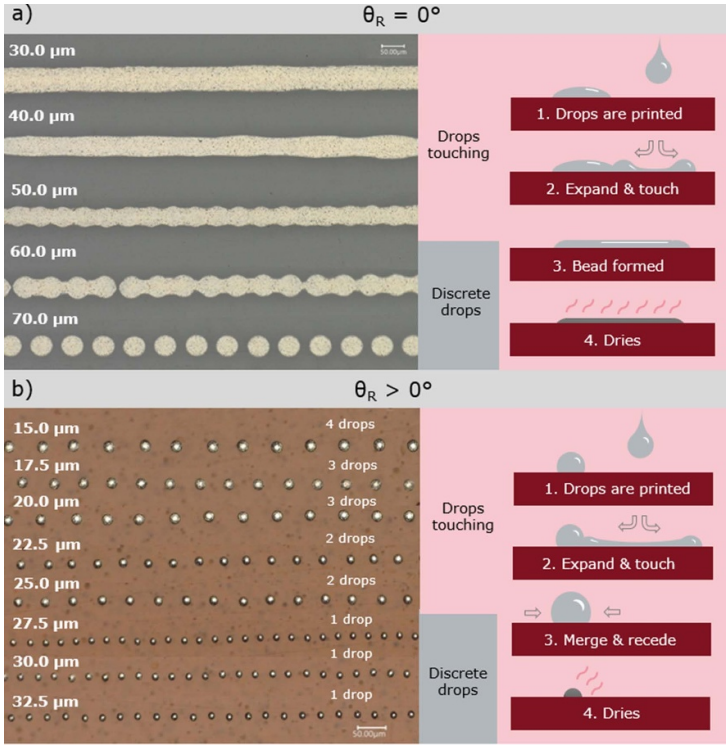

Figure 2. Prints with varying drop spacing (labeled) and the impact of θ_R on the bead formation. (a) The case of $\theta_A = 25.0°$ and $\theta_R = 0°$ for silver ink printed onto adhesion-coated PET, and (b) the case of $\theta_A = 82.7°$ and $\theta_R = 55.4°$ for silver ink printed onto FEP-coated polyimide.

17.5 μm result in the translation and coalescence of 3 adjacent drops into larger caps, and drops printed with spacing of 15.0 μm result in the translation and coalescence of 4 drops into a larger cap. As can be clearly seen, there is no value of drop spacing that results in the formation of a continuous line, because of the ability of the ink to recede on this substrate.

For the case of the drops printed on the Kapton FN substrate, which recede to form larger caps consisting of multiple coalesced drops, we would like to understand the position of the final coalesced caps relative to the positions of the originally printed drops. This can be determined clearly by examining the end of a printed line of drops, in which the last cap often consists of a separate, single drop, while the 2nd to last cap is often a coalesced drop containing multiple printed drops. This is shown for the case of lines printed with 20 μm drop spacing in figure 3 (one instance) and table 2 (4 separate instances). As shown, the diameters of the last caps are consistent with those of a single drop, while the diameters of the 2nd-to-last caps are consistent with those of 2 or 3 coalesced drops. We expect the last cap to remain at the position at which it was printed, because it consists of an isolated drop. However, we find that the center-to-center distances between the 2nd-to-last caps and the last caps are roughly 40 μm, which is twice the printed drop spacing of 20 μm. This suggests that for the

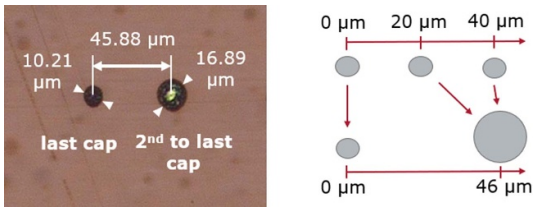

Figure 3. End of a printed line having 20 μm drop spacing, showing coalescence with backwards lateral translation.

caps consisting of coalesced drops, the drops that are printed later are moving back towards the drop that was printed first in that series, as shown schematically in the right side of figure 3. Similar behavior was observed in work by Schiaffino and Sonin while printing water on plexiglass, with the major difference being that here the center of the coalesced cap in our prints appears to be the center of the first drop in the series that coalesced [24].

We have seen that we cannot achieve continuous traces by printing normally with this ink on the Kapton FN substrate, but would still like to utilize the high θ_A of this ink-substrate combination to achieve narrow traces. Our approach is to first print a layer of 'seed' drops that are far enough apart (have a large enough drop spacing) such that they will not

Table 2. Measured size (diameter) and cap spacings at the ends of printed lines having 20 μm drop spacing.

	Last cap		2nd to last cap		
Trace	Size (μm)	# of drops	Size (μm)	# of drops	Observed spacing (μm)
1	11.89	1	17.11	2	38.38
2	11.82	1	17.91	2 or 3	38.97
3	10.21	1	16.87	2	45.88
4	11.79	1	15.75	2	42.63

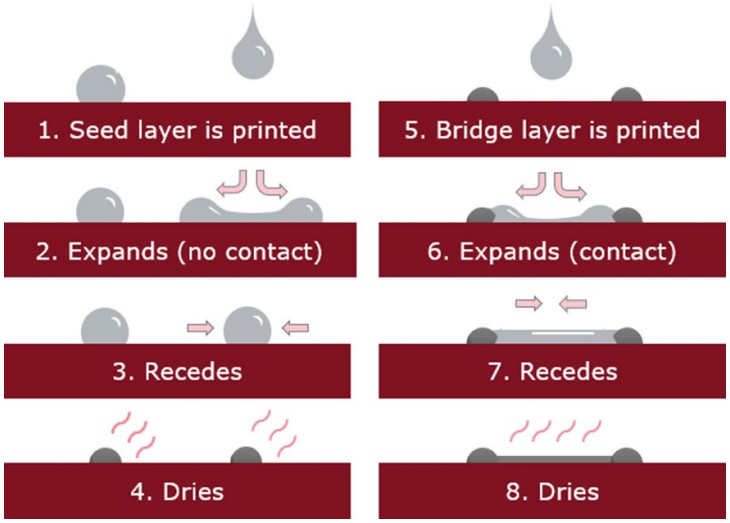

Figure 4. Illustration of the seed layer and bridge layer printing processes.

touch one another during the impact-driven expansion and will recede into a row of discrete drops. After these seed drops are dried, we print 'bridge' drops in between the seed drops so that the bridge drops are able to wet the dried seed drops during their impact-driven expansion and become pinned to the dried seed drops on both sides. Now, instead of receding into a small circular drop, the bridge drops will get pulled into a line, bridging the gap between the seed layer drops. This process is illustrated in figure 4 below. This requires that the drop spacing is both large enough so that the seed layer drops do not touch even during impact-driven expansion, but at the same time small enough that the bridge layer drops can touch both adjacent dried seed drops.

To choose the appropriate drop spacing for our prints, we need to know the diameter to which drops are expanding when they impact the substrate, so that we can properly space out the seed drops to prevent contact between adjacent seed drops. Due to the very small size of our 3.8 pl drops and the small 0.5 mm distance between the nozzles and the substrate, this expansion is very difficult to observe directly. Instead, by comparing the final distance between the observed drops on the substrate and the distance at which we printed each drop (the drop spacing), we can estimate the range of diameters to which the drops are expanding on impact. These measurements are plotted in figure 5 and are compared to the drop spacing and the diameter of the single 3.8 pl drop on the substrate.

In figure 5(a), we are comparing the observed cap spacing to the printed drop spacing. For small printed drop spacings, the cap spacing is larger than the drop spacing, indicating that the printed drops have coalesced into larger caps. At a drop spacing between 25.0 μm and 27.5 μm, the cap spacing becomes equal to the drop spacing, indicating that the printed drops are no longer coming into contact with one another and coalescing into larger caps, but are remaining separate. A similar conclusion is reached by comparing the cap diameter with the printed drop spacing, as shown in figure 5(b). Here, the cap diameter is very large for small drop spacings, indicating coalesced drops. The cap diameter decreases as the printed drop spacing is increased, indicating that fewer drops are coalescing to form each cap, until a printed drop spacing of between 25.0 and 27.5 μm, at which the cap diameter becomes a constant value, equal to the diameter of single printed drops that have not come into contact with another. By dividing the observed dried cap spacing by the printed drop spacing, we can estimate how many drops combined into each cap, as shown in figure 5(c). This tells us that 4 drops coalesce into a single cap for the smallest printed drop spacing of 15.0 μm, while single isolated drops are formed for

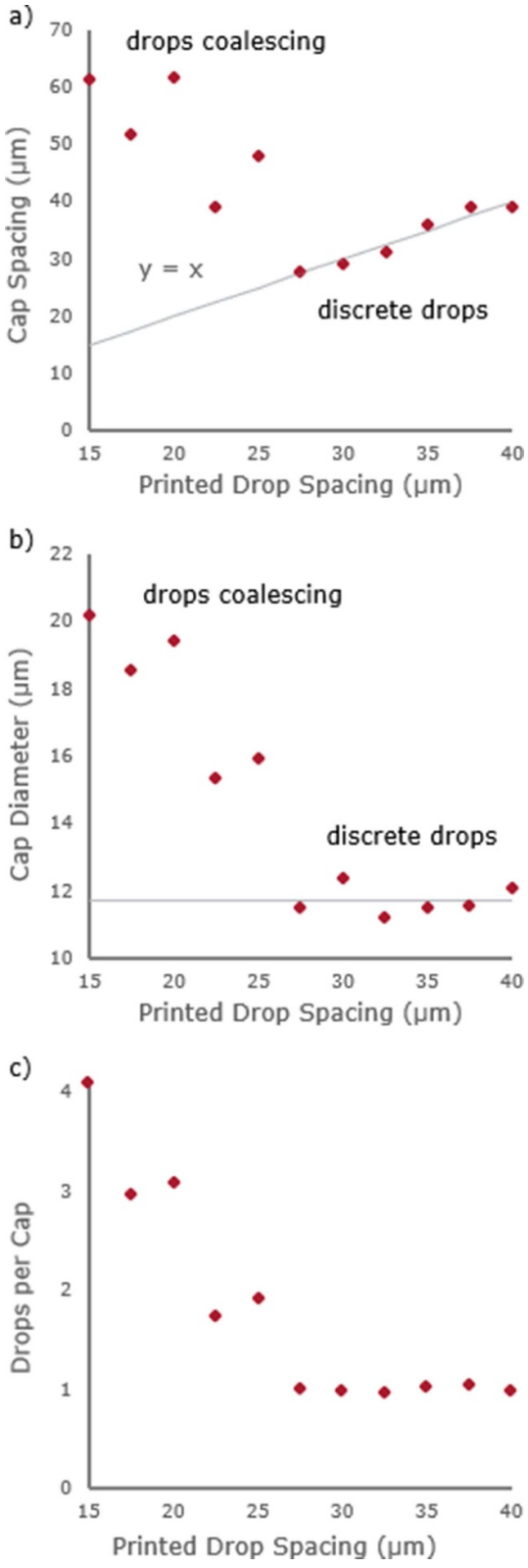

Figure 5. Coalescence of drops as a function of printed drop spacing: (a) cap spacing vs. printed drop spacing, (b) cap diameter vs. printed drop spacing, and (c) number of drops that have coalesced into the caps vs. printed drop spacing.

printed drop spacings larger than 27.5 μm. Therefore, 27.5 μm is the smallest printed drop spacing at which the drops will never come into contact with one another, despite impact-driven expansion. Knowing that the dried cap diameter is around 12 μm for single drops, and that the maximum drop spacing for coalescence is between 25.0 and 27.5 μm, we can now estimate the minimum and maximum possible diameter to which the drops are expanding upon impact with the substrate. If the previously printed drop is still at its maximum expansion when the next drop lands and expands, then the radius of expansion for the drops to touch is just half the drop spacing (i.e. a range of 12.5–13.75 μm). However, the previously printed drop may have already receded to a smaller diameter. This is described by t^*, which represents how far along the drop is in the expansion and recession process, and is shown below in equation (3) [26]

$$t^* = t\frac{V}{d_0}. \tag{3}$$

Here V is the drop velocity and t is time. Previous work estimates that the end of impact driven expansion occurs at around $t^* = 0.1$, and that the end of the recession and oscillation occurs between $t^* = 10$ and 100. For our drops this translates to ~0.35 μs for the end of impact driven expansion and between 0.035 and 0.35 ms for the end of the recession and oscillation. With adjacent drops being jetted with a delay of 1 ms (1 kHz jetting frequency), we would expect that the drop would have finished receding and oscillating before the next drop is placed. At this extreme, the previously printed drop has already expanded and receded to the final diameter of 12 μm by the time the next printed drop lands and expands. This means that the drop would need to have expanded to a radius equal to the drop spacing minus the dried cap radius (i.e. a range of 19–21.5 μm) in order to make contact with the previous drop. Therefore, from these experiments, we find that the drops are expanding to a radius in the range of 12.5–21.5 μm upon impact, with a radius closer to the higher end of this range being more likely.

Inkjet printing was then performed using one bitmap to print a line of drops for the seed layer, followed by offsetting this bitmap by half of the drop spacing to print the bridge layer drops in between the seed layer drops. We waited 10 min after printing the seed layer to print the bridge layer, to ensure that the seed layer was completely dry before the bridge layer was printed. This is purposefully excessive; we took drying measurements on larger drops, and estimated by converting the drying rate [27] to that of our smaller drops that it would take ~8.5 s for the 3.8 pl drop of ink to dry on the 70 °C surface, as shown in supplementary materials table S2 and figures S3, S4. For these seed-bridge prints we want to vary the drop spacing to find drop spacings at which the bridge drops touch the adjacent dried seed layer drops. For our lower limit we chose to print at 27.5 μm drop spacing for each layer, which (as described above) is the smallest spacing at which we expect the drops in each

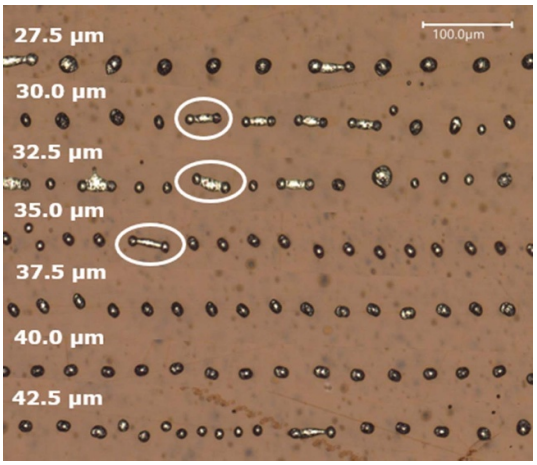

Figure 6. Printing with one pass each for the seed and bridge layers, with the labeled drop spacings. An example of successful bridging has been circled for each drop spacing.

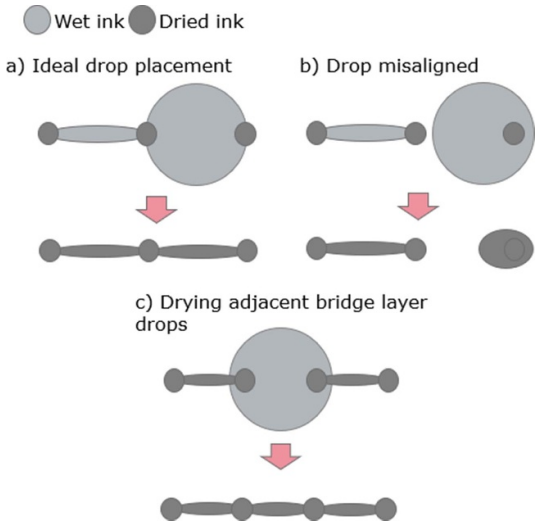

Figure 7. Influence of drop placement on wetting and final shape: (a), (b) printing with one pass for the seed and bridge layers; (c) printing the bridge layer in two passes and allowing the first one to dry before printing the second.

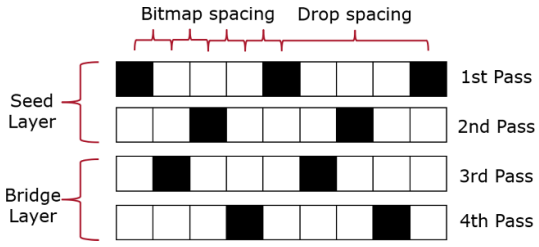

Figure 8. An illustration of the approach by which the bitmaps are split up into 4 print passes for seed and bridge printing.

layer to avoid coalescing (the spacing between adjacent seed layer and bridge layer drops would be half of this value, i.e. 13.75 μm). For the upper limit we chose to print at 42.5 μm drop spacing for each layer (again, with spacing between adjacent seed layer and bridge layer drops being half this value, i.e. 21.25 μm), at which we expect the seed and bridge layer drops to almost never touch, resulting in a series of discrete drops. These prints are shown below in figure 6.

With this print scheme we were unable to successfully print any continuous traces. At the larger drop spacings, the bridge layer drops generally wetted only one of the adjacent seed layer drops, or neither of them. At the smaller drop spacings the bridge layer drops were occasionally able to bridge both the seed layer drops on either side (especially for drop spacings of 30.0 and 32.5 μm), but more often were again only wetting one of the adjacent seed layer drops. The failure of this scheme to print continuous traces comes from limited drop placement accuracy, the impact of which is illustrated in figure 7 below. The error in the drop placement could come from variations in the drop jetting angle, variations in the drop volume, the mechanical accuracy of the stage of the LP50 printer (which is within a 5 μm range at 3 standard deviations) or a combination of all three.

The goal for this printing strategy was to print the drops as shown in figure 7(a), but what was largely observed was that the drops were misaligned and the bridge drops only wetted the seed layer cap on one side as shown in figure 7(b). To remedy this, we decided to split the bitmap up into four parts. This would allow us to print the drops closer together. By bringing the seed layer drops closer together, it will be easier to ensure that even if the bridge layer drop is misaligned due to positional inaccuracies, it will still wet the seed caps on both sides when it expands upon impact. To print the seed layer drops closer to one another, we need to print the seed layer in two passes so that the adjacent expanding drops cannot touch during printing. Similarly, we need to print the bridge layer drops in two passes so that we can dry the alternating bridge drops as shown in figure 7(c), which prevents the bridge drops from contacting and coalescing with wet ink from an adjacent bridge drop. The bitmaps were split up accordingly into 4 print passes as shown below in figure 8.

Again we varied the drop spacing for our prints. For the lower bound we chose 20 μm drop spacing, at which the drops in each layer will coalesce into large drops. For the upper bound we chose 120 μm drop spacing, so that the adjacent drops are 30 μm apart and the seed and bridge layers will never touch. As shown below in figure 9, we expect that the lower limit would result in the drops coalescing in each layer, and the upper limit would result in drops that never touch, even after all the layers have been printed.

The results for this print set are shown in figure 10(a), while a higher magnification image of a

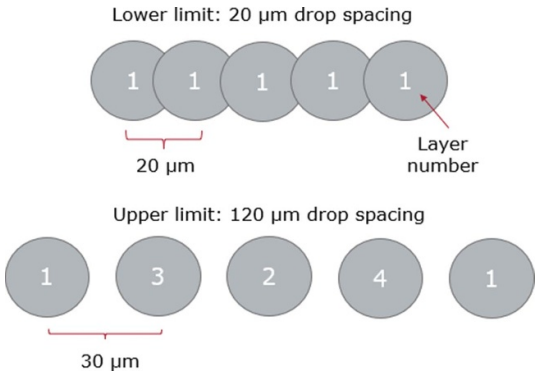

Figure 9. Lower and upper limit of drop spacing for the 4-layer seed-bridge print set.

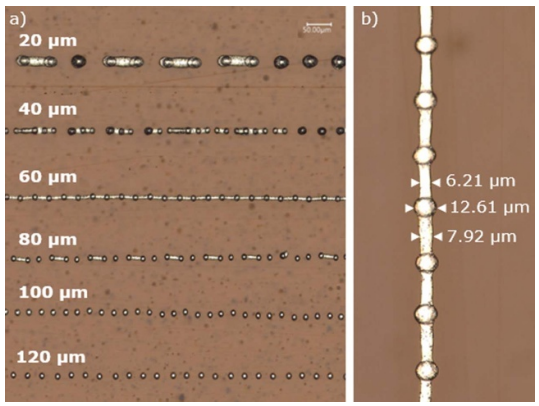

Figure 10. Results of seed and bridge layer printing in 4 passes: (a) prints with 20–120 μm drop spacing, (b) higher magnification image and measurements of continuous trace with 60 μm drop spacing.

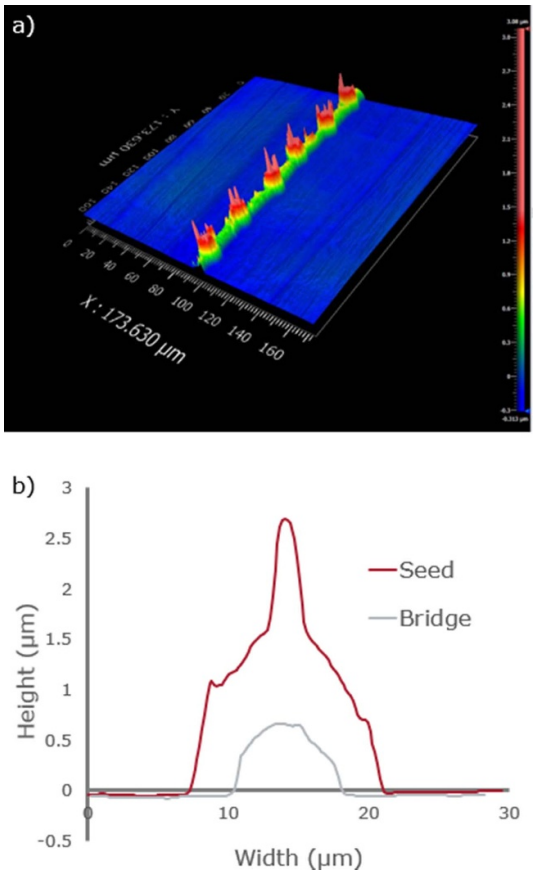

Figure 11. Profilometry of the continuous seed-bridge printed trace: (a) optical profile and (b) cross sections.

successfully-printed continuous trace having a drop spacing of 60 μm is shown in figure 10(b).

In these prints we can see the initial seed layer as the circular drops evenly spaced apart. As expected, the large drop spacings of 100 and 120 μm appear to be too far apart, with the bridge drops being visible as distinct drops between the seed layer drops. As the drop spacing is decreased, we start to see some bridging of the seed layer drops at 80 μm spacing, but it is not complete and we also see bridge drops which did not wet either of the seed layer drops. 60 μm drop spacing, on the other hand, results in long regions up to ~7 mm in length with continuous bridging between the seed layer drops. As shown in figure 10(b), this trace has a width of ~12.6 μm, which is equal to the diameter of the dried seed layer drops. At 40 μm drop spacing, in addition to the normally spaced drops, we see that some adjacent seed layer drops coalesced into larger drops. This is likely due to the drop spacing being mostly far enough apart from one another, but the variation of the drop placement still resulting in some drops that are too close to one another. Some of the bridge layer drops are spanning the seed layer drops, but in some locations we see that the bridge layer drops have coalesced around the seed layer drops. As expected for the 20 μm spaced prints, the seed layer drops appear to have coalesced into large drops spaced farther apart than printed. The bridge layer appears to have occasionally wetted both sides of the seed layer drops anyway, but there are also many instances in which it only wets one side, leaving the large drops.

Shown below in figure 11 is optical profilometry for the continuous printed trace having 60 μm drop spacing, along with the cross sections of a seed layer drop and the bridge.

We can see that the seed layer caps are the widest part of the trace, having a width of 12.6 μm, while the bridges are narrower, having a width between 6 and 8 μm. As expected, the cross-sectional area of the bridge is significantly smaller than for the seed caps.

The Agfa-Kapton FN ink-substrate combination with seed-bridge printing results in very narrow traces, but the adhesion of the trace to the substrate is very poor, to the extent that the traces are easily detached from the substrate by probes or tapes. To address this concern, we transferred the printed

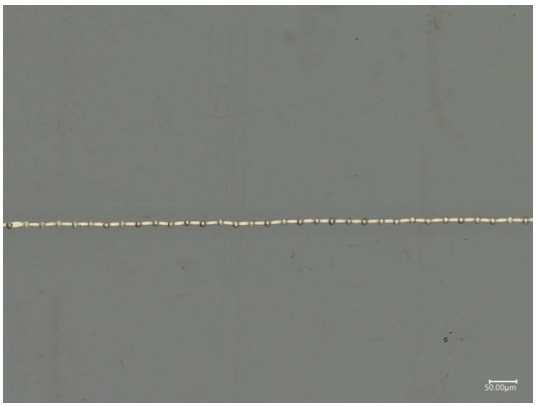

Figure 12. Seed-bridge trace transferred to PET ST505 substrate by hot pressing.

and annealed trace to a PET ST505 substrate, commonly used for printing, by hot pressing the PET onto the Kapton FN for 15 min at 250°F (121 °C) with an approximate pressure of ∼190 kPa (using a Vevor Heat Press Machine), followed by peeling it off. An optical image of the resulting trace after transferring to PET ST505 is shown in figure 12, and optical profilometry showing trace dimensions and shape is given in supplementary materials figures S5 and S6. The transferred trace has much better adhesion to the PET substrate. The profilometry shows that the transferred trace retains its cross-sectional widths, however the seeds appear to be only partially embedded in the PET substrate by the hot pressing, while the bridges seem to be suspended between the seeds. More work would need to be done to optimize this transfer process, perhaps by increasing the temperature and/or pressure, to fully embed the seeds into the PET substrate.

Electrical resistance is an important metric for inkjet-printed traces due to their relatively small cross-sectional areas. Electrical resistances of traces printed on Kapton FN (after curing at 170 °C for 30 min) were measured. Due to the small size and brittle nature of the traces (as well as the poor adhesion of the traces on the Kapton FN substrate), measuring the resistance using conventional probes was not feasible, as this resulted in damage or delamination. Instead, copper tapes were wetted with EGaIn eutectic liquid metal and gently pressed onto the traces to form an electrical contact. The length of the trace between the EGaIn contacts was then measured using microscope imaging. It should be noted that this is a destructive measurement, since the EGaIn dissolves the silver traces over time. Furthermore, as mentioned earlier, the longest continuous segments of the seed-bridge layer trace were relatively short (up to ∼7 mm length), and the EGaIn contacts are relatively large, therefore only 2-point resistance measurements were possible, rather than 4-point measurements, which would have been preferred to eliminate the influence of contact resistance. Instead, however, 2-point measurements were taken for different traces with different lengths as shown in supplementary materials figure S7 (plot of resistance vs. length), with the intention of fitting the data with a line and extrapolating to zero trace length to estimate both the resistance per length (slope) and the contact resistance (y-intercept). However, the resulting data points showed a large scatter, so that it is only possible to estimate that the resistance per trace length is in the range of 100–250 $\Omega\ \mathrm{mm}^{-1}$, and the contact resistance may be as large as 50 Ω.

For testing the electrical continuity of the traces before and after transfer, multiple straight parallel traces were printed next to one another on the Kapton FN substrate and then transferred to PET. For both the original traces and the transferred traces, copper tapes were wetted with EGaIn liquid metal and gently pressed onto the multiple parallel traces to form an electrical contact, images of which are shown in supplementary materials figure S8. In one instance, three parallel traces on Kapton FN had a resistance of 36 Ω, while two parallel traces transferred onto PET had a resistance of 26 Ω. As mentioned earlier, these are destructive measurements, so the measurements before and after transfer are performed on different trace samples. Additionally, a separate 4-point measurement on a film of the same printed silver material annealed at 170 °C for 30 min, showed that the resistivity decreases by less than 2% when it is exposed to additional annealing at 121 °C for 15 min, which is the temperature and time used for the transfer by hot pressing. Therefore, there is little or no decrease in resistance due to additional curing of the trace material during hot pressing.

4. Discussion

Trace width, trace spacing, printing speed, electrical resistance and trace length are all important considerations for inkjet printing. Regarding trace width, the 12.6 μm conductive trace width achieved here for the seed-bridge approach is significantly smaller than that achieved in previous work utilizing other methods to decrease the trace width for inkjet printing. The 79% reduction in trace width achieved by the seed and bridge layer printing method on Kapton FN relative to printing the same ink conventionally on PET ST505 is larger than the 71% reduction achieved by decreasing the drop volume [10], the 21% reduction from increasing the ink-substrate contact angle [19], and the 29% reduction achieved by increasing the drop spacing [18] that have been previously demonstrated in work on inkjet printing.

Regarding trace spacing, the decrease in trace width from 60 μm to 12.6 μm allows a significant

decrease (improvement) in minimum center-to-center trace spacing, and correspondingly a significant increase in trace density. However, when using the seed-bridge approach to print parallel traces next to each other with small spacing, for example as fingers on a sensor, one cannot consider only the final trace width to determine the minimum possible spacing, but must also consider the expansion and recession of the ink. For the common case that the drops in adjacent lines are not being jetted at the same time, the minimum spacing will be limited by the printed drop expanding out to touch the wet bridge layer in the adjacent lines. This spacing will be the radius of the expanded drop plus half the width of the wet seed layer trace. For our ink and substrate this will be a minimum center-to-center line spacing of $\sim$20 μm. If the lines are closer than this, the expanding drop will be able to wet the neighboring wet bridge drop, and those will again coalesce.

Regarding printing speed, the seed-bridge printing approach required four printing passes compared to the single pass required for other approaches. However, this is mitigated by the fact that fewer drops need to be jetted per pass in the seed-bridge approach because the drops within each pass do not overlap with one another, unlike in the single-pass approaches. As a specific comparison, for conventional 60 μm -wide traces printed here on PET ST505, we are printing a single layer with a drop spacing of 30 μm to achieve a $\sim$50% overlap of each drop with the previous drop, which is needed to print a smooth line with minimum trace width. However, for the seed-bridge approach, we are printing 4 layers, each with 60 μm drop spacing. If both approaches are printed at the same jetting frequency and if each pass in the seed-bridge approach is long enough that no additional wait time is needed in between passes for the ink to dry, then the seed-bridge approach would print at half the speed of the conventional approach. Note, however, that the seed-bridge approach would print 2.5 times faster than a hypothetical conventional single-pass approach in which the $\sim$12 μm -diameter discrete drops on Kapton FN are printed at 6 μm drop spacing to achieve 50% overlap.

Regarding electrical resistance, the observed differences in resistance are likely due to sample-to-sample variations. Therefore, these resistance values can only be used to conclude that the traces are electrically continuous as printed, and that this continuity is preserved after the transfer process. Additionally, the resistance per trace length of these seed-bridge traces (in the range of 100–250 $\Omega\,\mathrm{mm}^{-1}$) is likely to be sufficiently small only for very short traces, perhaps such as those used for the fingers of small interdigitated electrodes, or those used for the surface mount attachment of components with small and densely-spaced pads. The use of an ink with smaller volume resistivity would be needed to decrease the resistance further and enable the seed-bridge approach to be practical for longer traces. In addition, the accuracy and repeatability of inkjet drop placement position would need to be further improved to enable seed-bridge traces having longer continuous segments.

5. Conclusion

Typical strategies for reducing the width of inkjet-printed conductive traces run into issues with costs and time, either requiring additional processes to pattern the substrate or increasing ink deposition time. Increasing the advancing contact angle can bypass these issues but is limited in the impact it can have. If the contact angle is increased too much, then the ink can dewet the substrate and we can no longer stably print traces with a conventional approach. Here we have presented a strategy to print narrow continuous traces utilizing the ability of the printed ink to dewet certain substrates. Choosing an ink-substrate combination with $\theta_R > +0^\circ$ and printing and drying discrete seed drops allows us to print traces by connecting the dried drops of ink with bridge drops. The positional accuracy of the drops is more important in this approach than when printing conventional traces, but this can be mitigated by printing the seed drops in multiple layers. The traces can be transferred to another substrate while preserving electrical connectivity. The final traces demonstrated here have widths of 12.6 μm, which is the smallest width reported to date for stand-alone inkjet printing onto un-patterned substrates. Further improvements in drop-placement accuracy and repeatability are needed to enable seed-bridge traces with longer continuous segments and more consistent resistance per length, while further work is needed on the transfer process to fully embed the seeds of the traces in the PET substrate.

Data availability statement

All data that support the findings of this study are included within the article (and any supplementary files).

Funding

This material is based on research sponsored, in part, by Air Force Research Laboratory under Agreement Number FA8650-15-2-5401, as conducted through the flexible hybrid electronics manufacturing innovation institute, NextFlex. The U.S. Government is authorized to reproduce and distribute reprints for Governmental purposes notwithstanding any copyright notation thereon. The views and conclusions contained herein are those of the authors and should not be interpreted as necessarily representing

the official policies or endorsements, either expressed or implied, of Air Force Research Laboratory or the U.S. Government.

ORCID iDs

Nicholas Pratt https://orcid.org/0009-0005-2296-1149
Pratap M Rao https://orcid.org/0000-0003-1324-498X

References

[1] Wiklund A, Karako A, Palko T, Yiğitler H, Ruttik K, Jntti R and Paltakari J 2021 *J. Manuf. Mater. Process.* **5** 89
[2] Al-Halhouli A, Al-Ghussain L, El Bouri S, Habash F, Liu H and Zheng D 2020 *Appl. Sci.* **10** 480
[3] Fang Y, Hester J, Su W, Chow J, Sitaraman S and Tentzeris M 2016 *Sci. Rep.* **6** 39909
[4] Naik A *et al* 2022 *Lab Chip* **22** 156–69
[5] Georgas M, Selinis P, Zardalidis G and Farmakis F 2023 *IEEE Sens. J.* **23** 21–33
[6] Kawahara Y, Hodges S, Cook B, Zheng C and Abowd G *Proc. 2013 ACM Int. Joint Conf. on Pervasive and Ubiquitous Computing (Ubicomp '13)* pp 363–72
[7] Rosati G, Ravarotto M, Scaramuzza M, De Toni A and Paccagnella A 2019 *Sens. Actuators* B **280** 280–9
[8] Koskinen S, Pykäri L and Mäntysalo M 2013 *IEEE Trans. Compon. Packag. Manuf. Technol.* **3** 1604–10
[9] Abdolmaleki H, Kidmose P and Agarwala S 2021 *Adv. Mater.* **33** 2006792
[10] Meier H, Löffelmann U, Mager D, Smith P and Korvink J 2009 *Phys. Status Solidi* a **206** 1626–30
[11] Sekitani T, Noguchi Y, Zschieschang U, Klauk H and Someya T 2008 *Proc. Natl Acad. Sci.* **105** 4976–80
[12] Behera D and Cullinan M 2021 *Precis. Eng.* **68** 326–37
[13] Zikulnig J, Chang S, Bito J, Rauter L, Roshanghias A, Carrara S and Kosel J 2023 *Adv. Sens. Res.* **2** 2200073
[14] Stringer J and Derby B 2008 *J. Eur. Ceram. Soc.* **29** 913–8
[15] Hendriks C, Smith P, Perelaer J, van den Berg A and Schubert U 2008 *Adv. Funct. Mater.* **18** 1031–8
[16] Mei P, Ng T, Lujan R, Schwartz D, Kor S, Krusor B and Veres J 2014 *Appl. Phys. Lett.* **105** 123301
[17] Shrikanth V, Archana S and Bobji M 2019 *Meas. Sci. Technol.* **30** 075002
[18] Kim Y, Ren X, Kim J W and Noh H 2014 *J. Micromech. Microeng.* **24** 115010
[19] Yang J, Zheng F and Derby B 2021 *Langmuir* **37** 26–35
[20] Hemmilä S, Cauich-Rodríguez J, Kreutzer J and Kallio P 2012 *Appl. Surf. Sci.* **258** 9864–75
[21] Yeh K, Chen L and Chang J 2008 *Langmuir* **24** 245–51
[22] Whyman G, Bormashenko E and Stein T 2008 *Chem. Phys. Lett.* **450** 355–9
[23] Tadmor R 2004 *Langmuir* **20** 7659–64
[24] Schiaffino S and Sonin A 1997 *J. Fluid Mech.* **343** 95–110
[25] Duineveld P 2003 *J. Fluid Mech.* **477** 175–200
[26] Derby B 2010 *Annu. Rev. Mater. Sci.* **40** 395–414
[27] Hu H and Larson R 2002 *J. Phys. Chem. B* **106** 1334–44